Accepted Manuscript

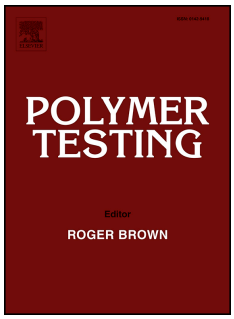

Loading rate dependence of failure strength as predictor for the long-term performance of thermoplastic polymeric products

Marc J.W. Kanters, Tim B. van Erp, Martin van Drongelen, Tom A.P. Engels, Leon E. Govaert

PII: S0142-9418(16)31440-4

DOI: 10.1016/j.polymertesting.2017.01.026

Reference: POTE 4912

To appear in: *Polymer Testing*

Received Date: 20 December 2016

Accepted Date: 29 January 2017

Please cite this article as: M.J.W. Kanters, T.B. van Erp, M. van Drongelen, T.A.P. Engels, L.E. Govaert, Loading rate dependence of failure strength as predictor for the long-term performance of thermoplastic polymeric products, *Polymer Testing* (2017), doi: 10.1016/j.polymertesting.2017.01.026.

Property Modelling

Loading rate dependence of failure strength as predictor for the long-term performance of thermoplastic polymeric products

Marc J.W. Kanters[a,d*], Tim B. van Erp[b], Martin van Drongelen[a,c], Tom A.P. Engels[a,d], Leon E. Govaert[a]

* Corresponding author. E-mail: marc.kanters@dsm.com

[a] Department of Mechanical Engineering, Materials Technology Institute, Eindhoven University of Technology, P.O.Box 513, 5600 MB, Eindhoven, The Netherlands
[b] SABIC Innovative Plastics B.V., P.O.Box 117, 4600 AC Bergen op Zoom, The Netherlands
[c] Present address: Production Technology Group, Faculty of Engineering Technology, University of Twente, Drienerlolaan 5, 7522 NB Enschede, The Netherlands
[d] Present address: DSM Ahead, Materials Sciences R&D, P.O.Box 18, 6160 MD Geleen, The Netherlands

ABSTRACT
An analytical methodology is presented that allows the prediction of long-term plasticity-controlled failure of statically loaded thermoplastic products. The only input required is the strength of the component obtained from short-term, load build-up experiments using various constant loading rates. The method is demonstrated by predicting the long-term performance based on short-term failure strength experiments of a number of materials for a simple geometry (uniaxial tensile bars), and a more complex geometry (internally pressurized pressure vessels).

KEYWORDS*:* strength, plasticity-controlled failure, plastic flow, polymeric products, short-term testing, long-term failure

1. INTRODUCTION

Due to low material and production costs, ease of processing, and freedom of design, polymers are increasingly employed in engineering applications. In many cases these applications are load-bearing and find their use at elevated temperatures. However, the most important problem encountered in such applications is that eventually all polymers will display time-dependent failure due to different failure mechanisms. Hence, to prevent premature failure in service, the ability to predict, or at the very least make estimates of, long-term performance is essential.

A common method to do so is by subjecting the actual product to temperatures and loads well above service conditions leading to short-term failure, similar to the classical testing of pipe grades according to ISO 1167 [1]. A linear regression of the resulting lifetime of the component as a function of the applied load offers the opportunity for extrapolation and estimation of the product's long-term service life. Although this seems a rather straight forward approach, it is difficult to estimate the applicable loading range beforehand; too low loads result in extreme long testing times, whereas too high loads result in almost immediate failure. Since the number of parts that can typically be tested is limited and the necessary experimental programs very time consuming (with failure times in the order of years), optimum use of both available samples and the experimental setup is crucial, i.e. prevent premature failure and run-outs. Therefore, for accurate lifetime estimations with limited resources, the availability of a short-term method that enables proper prediction of the outcome of the long-term test program is essential.

From previous efforts in developing predictive methods and work on pressurized polyethylene pipes in particular, it is known that there are three failure mechanisms that limit the lifetime of polymers under load: I) plasticity-controlled failure (creep rupture, delayed yielding), II) slow crack-growth, and III) molecular degradation [2],[3]. All three mechanisms act in parallel, creating three distinct regions in time where failure is dominated by one of them. In this work, the focus is on plasticity-controlled failure (Region I).

Plasticity-controlled failure is caused by the fact that, in solid polymers, the application of stress results in an increase of the molecular mobility [4]. In the case of a constant load, this results in a temperature and stress dependent constant plastic flow rate [5],[6] which, unfortunately, cannot be sustained indefinitely and eventually will lead to failure. Prediction of plasticity-controlled failure finds it origin in the experimental observation that the product of the time-to-failure and the strain rate at failure is constant for different loads [7],[8]. Combined with kinetic considerations, as proposed by Mindel and Brown [9], it is proven that the same holds for the product of the time-to-failure and the strain rate during secondary creep, and that the result of this multiplication can be regarded as a fictive critical strain at which failure occurs [10],[11]. Since the steady state during secondary creep is in fact identical to the state at the yield point during a constant rate experiment, as first demonstrated by Bauwens-Crowet et al. [5], the stress and temperature dependence of plastic flow can be fully characterized by that of the yield stress measured in well-defined, short-term constant strain rate experiments. This framework, combined with an Eyring based flow rule [6], has successfully been applied to predict time-to-failure for a multitude of polymers for various temperatures and loading conditions [10]-[16], simply by performing constant strain rate experiments to

determine the kinetics and short-term creep experiments to resolve the magnitude of the critical strain. For a more elaborate discussion on this approach, please refer to [10]-[13]. Unfortunately, it is nearly impossible to perform an experiment with constant strain rate on complex geometries (e.g. hydro blocks or engine mounts), whereas in these cases load controlled experiments are rather straight forward (e.g. internal pressure or load increase). Therefore, in the present paper, the framework discussed above is modified into an approach that predicts long-term plasticity-controlled failure of statically loaded polymeric products by using (short-term) failure strength experiments using various constant loading rates instead. The validity of the method is demonstrated on uniaxial tensile bars and internally pressurized pressure vessels for a number of materials.

2. EXPERIMENTAL

2.1 Materials

To check the universality of the approach several materials were used in this study, all kindly provided by SABIC. For the uniaxial tensile bars, three blends of polycarbonate LEXAN™ 141R resin with low temperature impact modifier, containing 0%, 4.5% and 9% by volume MBS, were used. Tensile bars were injection molded according to ISO 527 Type 1A using an Arburg 320S 500-150 ALLROUNDER™. For the pressure vessels, an unfilled NORYL™ 731S resin (NORYL), a 40% glass-filled NORYL™ GFN1740V resin (GFR NORYL), a rubber modified polycarbonate LEXAN™ ML3046 resin (rubber modified PC) and a PC siloxane copolymer LEXAN™ EXL1414T resin (PC) were used. Pressure vessels of all four materials were injection molded on a Krauss-Maffei KM200. Drying time and processing conditions were applied according to datasheet values.

2.2 Pressure vessel geometry

Glass fiber reinforced materials behave anisotropic, which implies non-identical properties in all directions. Therefore, well known properties like the Young's modulus and the tensile stress are dependent on the direction of load. Injection molded plastic products made from glass fiber reinforced material typically show a broad distribution of glass fiber orientation, as well as (multiple) knit lines throughout the product. To account for anisotropy in fiber reinforced materials, pressure vessels are used as test samples to probe the materials' performance in real applications.

The pressure vessel sample had the following properties (see
Figure 1):

- Two gate location options: 1) at the top resulting in a sample without weld line and 2) at the bottom creating a mild weld line along the length of the pressure vessel.
- The loading direction of the pressure vessel was perpendicular to the glass fiber orientation, causing a lower reinforcement effect compared to standard tensile bars.
- Average dimensions are length of 200 mm, inner diameter of 41.5 mm and wall thickness of 3 mm.

2.3 Uniaxial tensile experiments

Uniaxial tensile tests were performed at Eindhoven University of Technology using a Zwick Universal Testing Machine, equipped with a 10 kN load-cell. Failure strength tests, where the engineering stress increases linearly in time, were performed at room temperature and rates between 10^{-2} and 3 MPa/s until sudden neck formation. The maximum load was taken as failure strength. Creep measurements were performed for a wide range of applied engineering stresses and chosen such that the measurement times did not exceed 10^5 seconds. The stress was applied within 10 seconds and kept constant until failure. The time-to-failure was corrected for the load application time and was regarded to be the time when necking occurs.

2.4 Pressure vessels experiments

All pressure vessel experiments were performed at SABIC's Water Management Center of Excellence in Bergen op Zoom, the Netherlands. Burst pressure tests, where the pressure increases linearly in time and the pressure at rupture is obtained, were performed using an IPT Airless Professional Line model #1720, equipped with a 0-200 bar pressure-cell and a thermostatically controlled water bath. To characterize the deformation kinetics, burst pressure tests were performed at pressure rates ranging between 10^{-3} bar/s and 10^1 bar/s, while pressure was recorded as a function of time. Before starting the measurements, the samples were allowed to reach temperature equilibrium under water. All measurements were performed at least in duplicate. Creep rupture tests were performed using Regler RPCS - master III equipment with applied constant pressures in the range of 0-60 bar, and a thermostatically controlled water bath. The applied constant pressure loading levels ensured a wide variation of stresses, the ranges and temperatures being carefully chosen for each material in order to obtain failure in the time range between 10^2 and 10^6 s. Burst pressure and time-to-failure were determined by the pressure and time of rupture (loss of pressure), respectively.

3. THEORY

With failure occurring at a critical level of plastic strain, monitoring the accumulation of plastic strain over time enables calculation of time-to-failure with a time-dependent load, as in:

$$\bar{\varepsilon}_{pl}(t, \bar{\sigma}(t), T) = \int_0^t \dot{\bar{\varepsilon}}_{pl}(\bar{\sigma}(t'), T)\, dt' \qquad \text{with failure once} \qquad \bar{\varepsilon}_{pl} \geq \varepsilon_{cr} \qquad (1)$$

where $\bar{\varepsilon}_{pl}$ is the total amount of equivalent plastic strain accumulated over time, $\dot{\bar{\varepsilon}}_{pl}$ the equivalent plastic flow rate as function of equivalent stress and temperature, and ε_{cr} the critical strain at which failure occurs.

The kinetics of the equivalent plastic strain rate, $\dot{\bar{\varepsilon}}_{pl}$, and its dependence on stress- and temperature, is described using the pressure-modified Eyring relation according to Eyring's activated flow theory [6][17]:

$$\dot{\bar{\varepsilon}}_{pl}(\bar{\sigma},T) = \underbrace{\dot{\bar{\varepsilon}}_0(S)}_{I}\underbrace{\exp\left(-\frac{\Delta U}{RT}\right)}_{II}\underbrace{\sinh\left(\frac{\bar{\sigma}V^*}{kT}\right)}_{III}\underbrace{\exp\left(-\frac{\mu pV^*}{kT}\right)}_{IV} \tag{2}$$

where $\bar{\sigma}$ is the equivalent stress (here chosen as the Von Mises stress), p the hydrostatic pressure (both in $[Pa]$), V^* the activation volume in $[m^3]$, ΔU the activation energy in $[J/mol]$, μ the pressure dependence which is dimensionless, R the universal gas constant in $[J/mol/K]$, k the Boltzmann's constant in $[J/K]$, and T the (absolute) temperature in $[K]$.
One can identify various contributions in Equation (2); part (I) is a pre-exponential factor, $\dot{\bar{\varepsilon}}_0$, and is known to be related to the thermal history of the polymer [10]. The exponential term in part (II) covers the temperature dependence and part (III) the stress dependence of the material. Finally, the exponential term in part (IV) handles the effect of loading geometry via the hydrostatic pressure.
For sake of simplicity, when deriving the final expressions, Equation (2) is further reduced to:

$$\dot{\bar{\varepsilon}}_{pl}(\bar{\sigma},T) = \dot{\bar{\varepsilon}}_0^* \sinh\left(\frac{\bar{\sigma}}{\sigma_0}\right)\exp\left(-\frac{\mu p}{\sigma_0}\right) \tag{2}$$

with $\dot{\bar{\varepsilon}}_0^* = \dot{\bar{\varepsilon}}_0(S)\exp\left(-\frac{\Delta U}{RT}\right)$ and $\sigma_0 = \frac{kT}{V^*}$.

The definitions for the equivalent (plastic) strain rate, $\dot{\bar{\varepsilon}}_{pl}$, equivalent tensile stress, $\bar{\sigma}$, and hydrostatic pressure, p, are given in Table 1.

The derivation of the general expressions of i) the lifetime under constant load as function of applied load and ii) the maximum load as function of applied loading rate is illustrated for the situation of a uniaxial loading. By substituting the expressions of the equivalent stress and hydrostatic pressure in Equation (2) and using $\sinh(x) \approx \frac{1}{2}\exp(x)$ for $x \gg 1$ we obtain:

$$\dot{\bar{\varepsilon}}_{pl}(\sigma,T) = \frac{\dot{\bar{\varepsilon}}_0^*}{2}\exp\left(\frac{(\mu+3)}{3\sigma_0}\sigma\right) \tag{3}$$

3.1 Maximum load as function of applied loading rate applied

During load build-up experiments the stress is a function of time: $\sigma(t) = \dot{\sigma}\cdot t$. Hence, by combining Equation (1) and Equation (3), and substituting $\sigma(t) = \dot{\sigma}\cdot t$, the accumulated plastic strain in time as function of the applied stress rate is expressed as:

$$\bar{\varepsilon}_{pl}(t,\dot{\sigma},T) = \int_0^t \frac{\dot{\bar{\varepsilon}}_0^*}{2}\exp\left(\frac{(\mu+3)}{3\sigma_0}\dot{\sigma}\cdot t'\right)dt' \tag{4}$$

Integration of Equation (4) gives:

(5)

$$\bar{\varepsilon}_{pl}(t,\dot{\sigma},T) = \frac{3\dot{\bar{\varepsilon}}_0^*\sigma_0}{2(\mu+3)\dot{\sigma}}\left[\exp\left(\frac{(\mu+3)}{3\sigma_0}\dot{\sigma}\cdot t'\right)\right]_0^t$$

With failure occurring once a critical level of plastic strain has accumulated, i.e. $\bar{\varepsilon}_{pl} = \varepsilon_{cr}$, this relates to the time-to-failure via:

$$\begin{aligned}\varepsilon_{cr} &= \frac{3\dot{\bar{\varepsilon}}_0^*\sigma_0}{2(\mu+3)\dot{\sigma}}\left[\exp\left(\frac{(\mu+3)}{3\sigma_0}\dot{\sigma}\cdot t'\right)\right]_0^{t_f} \\ &= \frac{3\dot{\bar{\varepsilon}}_0^*\sigma_0}{2(\mu+3)\dot{\sigma}}\left[\exp\left(\frac{(\mu+3)}{3\sigma_0}\dot{\sigma}\cdot t_f\right)-1\right]\end{aligned} \tag{6}$$

At failure, the maximum stress σ_f, is equal to the product $\dot{\sigma}\cdot t_f$, thus, for significantly large rates, this relation can be further reduced to provide the maximum stress as a function of stress rate:

$$\sigma_f = \dot{\sigma}\cdot t_f = \underbrace{\frac{3\sigma_0}{(\mu+3)}}_{\alpha_{1,ut}}\ln(\dot{\sigma}) + \underbrace{\frac{3\sigma_0}{(\mu+3)}\ln\left(\frac{2(\mu+3)\varepsilon_{cr}}{3\dot{\bar{\varepsilon}}_0^*\sigma_0}\right)}_{\alpha_{2,ut}} \tag{7}$$

Thus, the loading rate dependence of the failure strength is defined by regression constants $\alpha_{1,ut}$ and $\alpha_{2,ut}$.

3.2 Time-to-failure in static loading

Similar as for the load build-up, for a constant load, the accumulated plastic strain in time as function of the load applied, σ_{app}, is defined by Equation (1) and (3) and linked to the time-to-failure, via the critical strain:

$$\bar{\varepsilon}_{pl}(t_f,\sigma_{app},T) = \int_0^{t_f}\frac{\dot{\bar{\varepsilon}}_0^*}{2}\exp\left(\frac{(\mu+3)}{3\sigma_0}\sigma_{app}\right)dt' = \varepsilon_{cr} \tag{8}$$

Therefore, the time-to-failure relates to the applied load according to:

$$t_f = \frac{2\bar{\varepsilon}_{cr}}{\dot{\bar{\varepsilon}}_0^*}\exp\left(-\frac{(\mu+3)}{3\sigma_0}\sigma_{app}\right) \tag{9}$$

which shows that the applied load versus time-to-failure is given by:

$$\begin{aligned}\sigma_{app} &= -\frac{3\sigma_0}{(\mu+3)}\ln(t_f) + \frac{3\sigma_0}{(\mu+3)}\ln\left(\frac{2\varepsilon_{cr}}{\dot{\bar{\varepsilon}}_0^*}\right) \\ &= -\frac{3\sigma_0}{(\mu+3)}\ln(t_f) + \frac{3\sigma_0}{(\mu+3)}\ln\left(\frac{3\sigma_0}{(\mu+3)}\right) \\ &\quad + \frac{3\sigma_0}{(\mu+3)}\ln\left(\frac{2\varepsilon_{cr}}{\dot{\bar{\varepsilon}}_0^*}\frac{(\mu+3)}{3\sigma_0}\right)\end{aligned} \tag{10}$$

Or, once more, in terms of $\alpha_{1,ut}$ and $\alpha_{2,ut}$:

$$\sigma_{app} = -\alpha_{1,ut} \ln(t_f) + \alpha_{1,ut} \ln(\alpha_{1,ut}) + \alpha_{2,ut} \tag{11}$$

This implies that failure strength experiments conducted at various loading rates offer sufficient information to determine α_1 and α_2 using a simple linear regression model, where α_1 is the slope and α_2 the value at a loading rate of 1 MPa/s, which can directly be used to predict the long-term failure of statically loaded samples.

4. Results and Discussion

4.1 Application on uniaxial tensile bars: predicting the lifetime

The equations derived to describe the failure strength of uniaxial tensile bars and predict the time-to-failure for a constant load experiment are applied for PC with 0%, 4.5% and 9% by volume MBS in Figure 2. This figure shows that the kinetics are identical for all the polycarbonates, but a decrease in stress is found with increasing MBS content. As can be seen in Figure 2b, the resulting regression constants from the stress rate dependence of the burst stress in Figure 2a enables a good prediction of the stress dependence of the time-to-failure, although the lifetime is slightly overestimated. This minor overestimation is related to differences in the average true stress during these experiments, since the strain evolution as a function of time differs for each experiment. However, in most of the load controlled experiments, such as the pressure vessels, no strain information is available and true stress conditions cannot be derived. Therefore, one is forced to work with engineering values, which still yield an accurate prediction that can be used to estimate, for example, the applicable loading range.

4.2 Application on pressure vessels: deriving the expressions

To illustrate the general applicability of this approach, it is also derived and demonstrated on pressure vessels. For end-capped pressure vessels, the expressions for the equivalent stress and hydrostatic pressure are:

$$\bar{\sigma} = \frac{\sqrt{3}}{2}\sigma_h = \frac{\sqrt{3}(D-2t)p_i}{4t} \tag{12}$$

$$p = -\frac{1}{2}\sigma_h = -\frac{(D-2t)p_i}{4t} \tag{13}$$

where D and t are the diameter and the wall thickness of the pressure vessels, respectively, and p_i is the internal pressure.

Substitution of these expressions into Equation (2) and using a derivation similar as presented in the Theory section, yields the internal pressure at failure, $p_{i,f}$, as a function of the constant pressure build up rate, $\dot{p}$, provided by:

$$p_f = \alpha_{1,pv} \ln(\dot{p}) + \alpha_{2,pv} \tag{14}$$

wherein $\alpha_{1,pv} = \frac{4t\sigma_0}{(\mu+\sqrt{3})(D-2t)}$ and $\alpha_{2,pv} = \frac{4t\sigma_0}{(\mu+\sqrt{3})(D-2t)} \ln\left(\frac{\bar{\varepsilon}_{cr}(\mu+\sqrt{3})(D-2t)}{2t\sigma_0 \dot{\bar{\varepsilon}}_0^*}\right)$

and for a constant applied internal pressure, $p_{i,app}$, as function of the time-to-failure:

$$p_{i,app} = -\alpha_{1,pv} \ln(t_f) + \alpha_{1,pv} \ln(\alpha_{1,pv}) + \alpha_{2,pv} \tag{15}$$

This clearly shows that the relation between load build-up and constant load experiments is exactly the same for pressure vessels as for uniaxial tensile bars, albeit that the expressions for the regression constants α_1 and α_2 slightly differ. Indeed, one should note that this holds for any stress state, as long as it is the same for both type of experiments and plasticity-controlled failure is addressed.

4.3 Application on pressure vessels: predicting the lifetime

Figure 3 shows the application of Equations (14) and (15) on internally pressurized pressure vessels produced from a 4% rubber modified polycarbonate (PC). As can be seen, the values for α_1 and α_2 obtained from the fit on the data in Figure 3a result in an accurate description of both short-term (Figure 3a) and long-term failure data (Figure 3b). However, unfortunately, the creep rupture experiments with an internal pressure applied below 40 bar show brittle failure related to crack-growth [2][3]. Since the provided approach only covers failure in the plasticity-controlled regime, this regime cannot be described using the parameters determined.

To further validate this method, burst pressure tests were also performed on glass-filled NORYL. Please note that, although this material displays failure in a rather brittle manner, i.e. at small macroscopic strains, this does not necessarily mean that failure is crack-growth controlled and, also in this case, the actual mechanism causing failure is still related to accumulation of plastic strain [12]. As Figure 4 shows, this method provides an excellent prediction for this grade, which proves this to be a useful method to estimate the lifespan of the material beforehand.

4.4 Including the temperature dependence

Finding its base in the theory of absolute reaction rates, the regression parameters can easily be adapted to also include the influence of temperature. According to the Eyring flow theory, temperature affects two terms: the stress dependency, characterized by the activation volume, V^*, and the temperature dependence of the pre-exponential factor $\dot{\bar{\varepsilon}}_0^*$, containing the activation energy ΔU. In the simplified form, both these terms are included in α_1 and α_2, thus to do so, the absolute temperature, T, has to be extracted from different terms in the model, as explained in Appendix A. This results in:

$$p_{i,f} = T\beta_{1,pv} \ln(\dot{p}) + T\beta_{1,pv} \ln\left(\beta_{2,pv} \exp\left(\frac{\beta_{3,pv}}{T}\right) \frac{1}{T\beta_{1,pv}}\right) \tag{16}$$

and for the applied stress as function of time-to-failure:

(17)

$$p_{i,app} = -T\beta_{1,pv}\ln(t_f) + T\beta_{1,pv}\ln(T\beta_{1,pv}) + T\beta_{1,pv}\ln\left(\beta_{2,pv}\exp\left(\frac{\beta_{3,pv}}{T}\right)\frac{1}{T\beta_{1,pv}}\right)$$

where $\beta_{1,pv} = \frac{4tk}{(\mu+\sqrt{3})(D-2t)V^*}$, $\beta_{2,pv} = \frac{2\varepsilon_{cr}}{\dot{\varepsilon}_0(S)}$, and $\beta_{3,pv} = \frac{\Delta U}{R}$.

This seems to complicate the issue, however, it is still rather simple to determine these three parameters using any mathematical program which can make a linear regression, as also illustrated in Appendix A.

Equations (16) and (17) are applied on the burst pressures of polycarbonate obtained at different temperatures and, as shown in Figure 5, this gives an accurate description of the time-to-failure at different temperatures. However, note that at longer times and high temperature failure is again controlled by slow crack growth.

To further substantiate this proposed approach, this method was also applied on a NORYL resin grade. However, as shown in Figure 6a, the burst pressures at different temperatures show a decrease in the rate dependence with increasing temperature, whereas, according to the Eyring theory, the slope should actually increase with increasing temperature. This is indicative of the contribution of an additional molecular process to the deformation process [18][20], e.g. a (secondary) glass transition (partial main-chain or side-chain mobility), easily recognized in a DMTA experiment. However, it is known that the long-term behavior is determined by a process active at high temperatures and lower rates [13][16]. If all the data points would be considered in the linear regression, the outcome would be a too steep slope (high α_1) and an underestimation of the performance at longer times results. In order to capture the process that determines the long-term performance, one should focus on the high temperature and low pressure rate data to determine the regression parameters. Therefore, the high pressure rate and low temperature data is neglected, as indicated with the gray inset in Figure 6a, and, as shown in Figure 6b, this gives an accurate description of the time-to-failure at different temperatures.

Studying the evolution of the regression constants for different geometries and materials lies beyond the scope of this paper, but one should keep in mind that the regression constants contain the parameters from the Eyring flow rule. In other words, one can use reported parameters and trends using the Eyring theory to complement the presented method, for example using some of the references addressed in the introduction section. This paper shows the general applicability of this straight forward method to predict the performance in long-term constant load experiments of different geometries using the strength measured during load build-up experiments.

5. CONCLUSIONS

An analytical model is provided that translates short-term, load build-up experiments with a constant loading rate to long-term plasticity-controlled failure under a static load. A linear regression of the maximum load versus load build-up rate provides sufficient information to predict the long-term performance.

The model is derived for two different loading geometries, tensile bars and pressure vessels, indicating the method is generic and applicable to any arbitrary geometry, as long as both experiments are performed on the same sample geometry. Furthermore, being based on Eyring flow theory, the formulations can easily be modified to also incorporate the influence of temperature. The model is verified on uniaxial tensile bars and injection molded pressure vessels of different materials, which shows that the burst pressure can be directly related to the lifetime in creep experiments.

6. ACKNOWLEDGEMENTS
The authors gratefully acknowledge Erik Stam for his support from the SABIC Water Management Center of Excellence, Bergen op Zoom, The Netherlands.

7. APPENDIX A: INCLUDING THE TEMPERATURE DEPENDENCE
According to the Eyring flow theory temperature affects two terms: the stress dependency, characterized by the activation volume, V^*, and the temperature dependence of the pre-exponential factor $\dot{\varepsilon}_0^*$, containing the activation energy ΔU. In the simplified form both these terms are included in α_1 and α_2, thus the temperature dependence of these parameters can be used to include the temperature dependence. This can be done by extracting the absolute temperature, T, via:

$$\alpha_{1,pv} = \beta_{1,pv} T, \text{ with } \beta_{1,pv} = \frac{4tk}{(\mu+\sqrt{3})(D-2t)V^*} \tag{A1}$$

$$\alpha_{2,pv} = \beta_{1,pv} T \ln\left(\beta_{2,pv} \exp\left(\frac{\beta_{3,pv}}{T}\right)\frac{1}{\beta_{1,pv} T}\right), \text{ with } \beta_{2,pv} = \frac{2\varepsilon_{cr}}{\dot{\varepsilon}_0(S)}, \text{ and } \beta_{3,pv} = \frac{\Delta U}{R}. \tag{A2}$$

Note that in this case it is illustrated for pressure vessels, although for the sake of clarity the subscript pv is omitted, but this temperature dependence is the same for all geometries.

Although the expressions in Equation (A1) and (A2) appear a lot more complicated, $\beta_{1,pv}, \beta_{2,pv}$ and $\beta_{3,pv}$ can easily be determined. First find $\alpha_{1,pv}$ and $\alpha_{2,pv}$ for different temperatures using the linear relations for the maximum load as function of applied loading rate as in Equation (14). The value of $\beta_{1,pv}$ is found by taking the mean value of the different slopes corrected for temperature:

$$\beta_{1,pv} = \frac{{}^{\alpha_{1,T_1}}/_{T_1} + {}^{\alpha_{1,T_2}}/_{T_2} + \cdots + {}^{\alpha_{1,T_n}}/_{T_n}}{n} \tag{A3}$$

However, even though the value of $\beta_{1,pv}$ is not expected to vary significantly for different temperatures, the experimental error might cause minor deviations in its absolute value.

Therefore, once taken the average, it requires an update of α_2 for each temperature for that specific value, here taken as $\alpha_2'(T)$:

$$\begin{aligned}\alpha_2'(T) &= mean\left(p_{i,f}(T) - \beta_{1,pv} T \ln\left(\dot{p}(T)\right)\right) \\ &= \beta_{1,pv} T \ln\left(\beta_{2,pv} \exp\left(\frac{\beta_{3,pv}}{T}\right)\frac{1}{\beta_{1,pv} T}\right)\end{aligned} \tag{A4}$$

where α_2' is the offset for each temperature corresponding with the data using the average value for $\beta_{1,pv}$.

The values for $\beta_{2,pv}$ and $\beta_{3,pv}$ are easily obtained by rewriting the expression presented in Equation (A2), such that all the unknown terms are expressed as function of $1/T$.

$$\ln\left[\beta_{1,pv} T \cdot \exp\left(\frac{\alpha_2'(T)}{\beta_{1,pv}\mathrm{T}}\right)\right] = \frac{1}{T}\beta_{3,pv} + \ln\left(\beta_{2,pv}\right) \tag{A5}$$

Subsequently, the terms for the other parameters follow from the linear fit of this left hand term versus the reciprocal of temperature, $\frac{1}{T}$, see Figure A1 where this is illustrated for the case of PC presented in Figure 5. Here the two constant result from $\beta_{2,pv} = \exp(b)$ and $\beta_{3,pv} = a$, where a and b are the slope and offset from the linear regression respectively.

8. REFERENCES

[1] ISO 1167 Plastics pipes for the transport of fluids - Determination of the resistance to internal pressure".

[2] U.W. Gedde, J. Viebke, H. Leijström, M. Ifwarson, Long-term properties of hot-water polyolefin pipes e a review, Polym. Eng. Sci. 34 (24) (1994) 1773-1787.

[3] R.W. Lang, A. Stern, G. Doerner, Applicability and limitations of current lifetime prediction models for thermoplastics pipes under internal pressure, Die Angew. Makromol. Chem. 247 (1) (1997) 131-145.

[4] L.S. Loo, R.E. Cohen, K.K. Gleason, Chain mobility in the amorphous region of nylon 6 observed under active uniaxial deformation, Science 288 (5463) (2000) 116-119.

[5] C. Bauwens-Crowet, J.M. Ots, J.C. Bauwens, The strain-rate and temperature dependence of yield of polycarbonate in tension, tensile creep and impact tests, J. Mater. Sci. 9 (7) (1974) 1197-1201.

[6] H. Eyring, Viscosity, plasticity, and diffusion as examples of absolute reaction rates, J. Chem. Phys. 4 (4) (1936) 283-291.

[7] J.M. Crissman, G.B. McKenna, Relating creep and creep rupture in PMMA using a reduced variable approach, J. Polym. Sci. Pol. Phys. 25 (8) (1987) 1667-1677.

[8] E.J. Kramer, E.W. Hart, Theory of slow, steady state crack growth in polymer glasses. Polymer, 25 (1984) 1667-1678.

[9] M.J. Mindel, N. Brown, Creep and recovery of polycarbonate. J. Mat. Sci., 8 (1973) 863-870.

[10] H.A. Visser, T.C. Bor, M. Wolters, T.A.P. Engels, L.E. Govaert, Lifetime assessment of load-bearing polymer glasses: an analytical framework to ductile failure, Macromol. Mater. Eng. 295 (7) (2010) 637-651.
[11] T.B. van Erp, C.T. Reynolds, T. Peijs, J.A.W. van Dommelen, L.E. Govaert, Prediction of yield and long-term failure of oriented polypropylene: kinetics and anisotropy, J. Polym. Sci. Pol. Phys. 47 (20) (2009) 2026-2035.
[12] M.J.W. Kanters, T. Kurokawa, L.E. Govaert, Competition between plasticity-controlled and crack-growth controlled failure in static and cyclic fatigue of thermoplastic polymer systems. Pol. Testing 50 (2016) 101-110
[13] M.J.W. Kanters, K. Remerie, L.E. Govaert. A New Protocol for Accelerated Screening of Long-Term Plasticity-Controlled Failure of Polyethylene Pipe Grades. Pol. Eng. Sci, 56 (6) (2016) 676-688.
[14] T.A.P. Engels, S.H.M. Söntjens, T.H. Smit, L.E. Govaert, Time-dependent failure of amorphous polylactides in static loading conditions, J. Mater. Sci. Mater. M. 21 (1) (2010) 89-97.
[15] R.P.M. Janssen, L.E. Govaert, H.E.H. Meijer, An analytical method to predict fatigue life of thermoplastics in uniaxial loading: sensitivity to wave type, frequency, and stress amplitude, Macromolecules 41 (7) (2008) 2531-2540.
[16] T.B. van Erp, D. Cavallo, G.W.M. Peters, L.E. Govaert, Rate-, temperature-, and structure-dependent yield kinetics of isotactic polypropylene, J. Polym. Sci. Pol. Phys. 50 (20) (2012) 1438-1451.
[17] I.M. Ward, Review: The yield behaviour of polymers. J. Mat. Sci., 1971. 6, 1397-1417.
[18] T. Ree, H. Eyring, Theory of non-Newtonian flow. I. Solid plastic system, J. Appl. Phys. 26 (7) (1955) 793-800.
[19] J.A. Roetling, Yield stress behaviour of polymethylmethacrylate, Polymer 6 (6) (1965) 311-317.
[20] C. Bauwens-Crowet, J.C. Bauwens, G. Homès, Tensile yield-stress behavior of glassy polymers, J. Polym. Sci. A2 7 (4) (1969) 735-742.

9. FIGURE CAPTIONS

Figure 1: *Gating options, weld line location and glass fiber orientation in a pressure vessel sample.*

Figure 2: *Data and predictions on uniaxial tensile bars of different rubber modified PC grades. (a) Failure strength versus the applied stress rate. (b) Time-to-failure data for different applied stresses. Markers represent measurement data; lines the model of Equation (7) and (11) using the parameters presented in Table 2.*

Figure 3: *Data and predictions on pressure vessels of rubber-filled PC at 60°C. (a) Burst pressure versus the applied pressure rate. (b) Time-to-failure data for different applied pressures. Markers represent plasticity-controlled failure (open symbols) and crack-growth controlled failure (filled symbols); lines represent the model of Equation (14) and (15) using the parameters provided in Table 3.*

Figure 4: *Data and predictions on pressure vessels of glass-filled NORYL at 60°C and 90°C. (a) Burst pressure versus the applied pressure rate. (b) Time-to-failure data for different applied pressures. Markers represent data; lines represent the model of Equation (14) and (15) using the parameters provided in Table 3.*

Figure 5: *Data and predictions on pressure vessels of polycarbonate at 40°C, 60°C and 90°C. (a) Burst pressure versus the applied pressure rate. (b) Time-to-failure data for different applied pressures. Markers represent data; lines represent the model of Equations (16) and (17) using the parameters provided in Table 4.*

Figure 6: *Data and predictions on pressure of NORYL resin at several temperatures. (a) Burst pressure versus the applied pressure rate. (b) Time-to-failure data for different applied pressures. Markers represent data; lines represent the model of Equations (16) and (17) using the parameters provided in Table 4.*

Figure A1: *Application of the linear regression presented in Equation (A5) on the data of PC in Figure 5. Markers represent values for different temperatures, the line the corresponding linear regression providing* β_2 *and* β_3*.*

10. TABLES

Definition	Tens.	Comp.	Shear
$\dot{\bar{\varepsilon}}_{pl} = \frac{\sqrt{2}}{3}\sqrt{(\dot{\varepsilon}_{11}-\dot{\varepsilon}_{22})^2+(\dot{\varepsilon}_{22}-\dot{\varepsilon}_{33})^2+(\dot{\varepsilon}_{33}-\dot{\varepsilon}_{11})^2+6(\dot{\varepsilon}_{12}^2+\dot{\varepsilon}_{23}^2+\dot{\varepsilon}_{13}^2)}$	$\dot{\varepsilon}$	$\dot{\varepsilon}$	$\frac{\dot{\gamma}}{\sqrt{3}}$
$\bar{\sigma} = \frac{\sqrt{2}}{2}\sqrt{(\sigma_{11}-\sigma_{22})^2+(\sigma_{22}-\sigma_{33})^2+(\sigma_{33}-\sigma_{11})^2+6(\sigma_{12}^2+\sigma_{23}^2+\sigma_{13}^2)}$	σ	σ	$\sqrt{3}\tau$
$p = -\frac{1}{3}(\sigma_{11}+\sigma_{22}+\sigma_{33})$	$-\frac{1}{3}\sigma$	$\frac{1}{3}\sigma$	0

Table 1: *Definitions of the equivalent Von Mises plastic strain rate, $\dot{\bar{\boldsymbol{\varepsilon}}}_{\boldsymbol{pl}}$, stress, $\bar{\boldsymbol{\sigma}}$, and hydrostatic pressure, $\boldsymbol{p}$, expressed in components of the deformation and stress tensor, respectively, and the explicit expressions for tension, compression and shear.*

Material	$\alpha_{1,ut}$	$\alpha_{2,ut}$
PC 0% MBS	1.10	63.40
PC 4.5% MBS	1.07	59.63
PC 9% MBS	1.09	55.65

Table 2: *Regression constants used in Equation (7) and (11) for the data of different rubber modified PC grades presented in Figure 2.*

Material	$\alpha_{1,pv}$	$\alpha_{2,pv}$
rubber modified PC	1.83	64.83
GFR NORYL resin	3.16	62.31

Table 3: *Regression constants used in Equation (14) and (15) for the data of rubber modified PC and GFR NORYL resin presented in Figure 3 and Figure 4 respectively.*

Material	$\beta_{1,pv}$	$\beta_{2,pv}$	$\beta_{3,pv}$
PC	0.0049	$5.6 \cdot 10^{-37}$	$4.09 \cdot 10^{4}$
NORYL	0.0035	$1.3 \cdot 10^{-46}$	$4.67 \cdot 10^{4}$

Table 4: *Regression constants used in the temperature dependent description (Equation (16) and (17)) for the data of PC and NORYL resin presented in Figure 5 and Figure 6 respectively.*

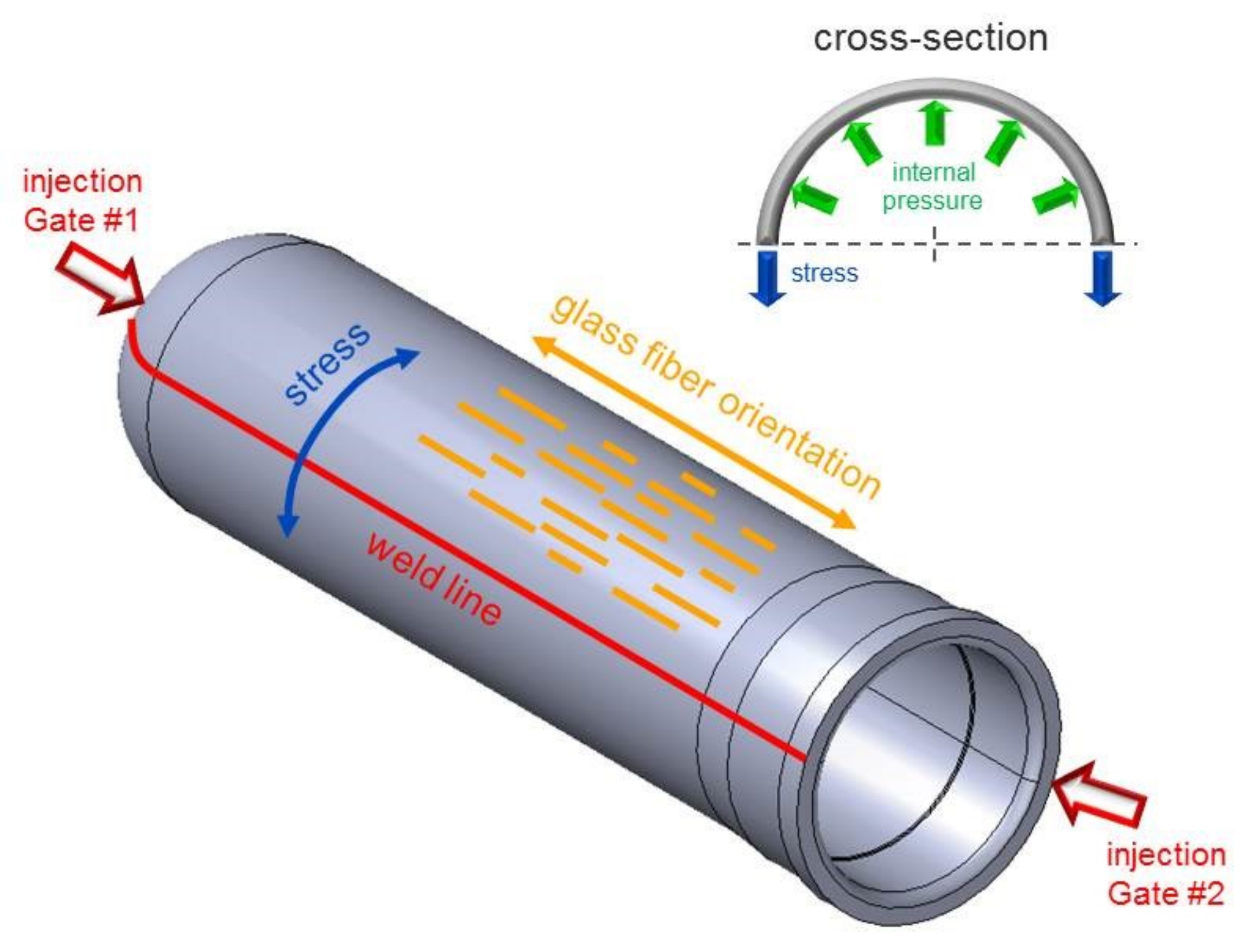
cross-section
internal
pressure
stress
injection
Gate #1
stress
glass fiber orientation
weld line
injection
Gate #2

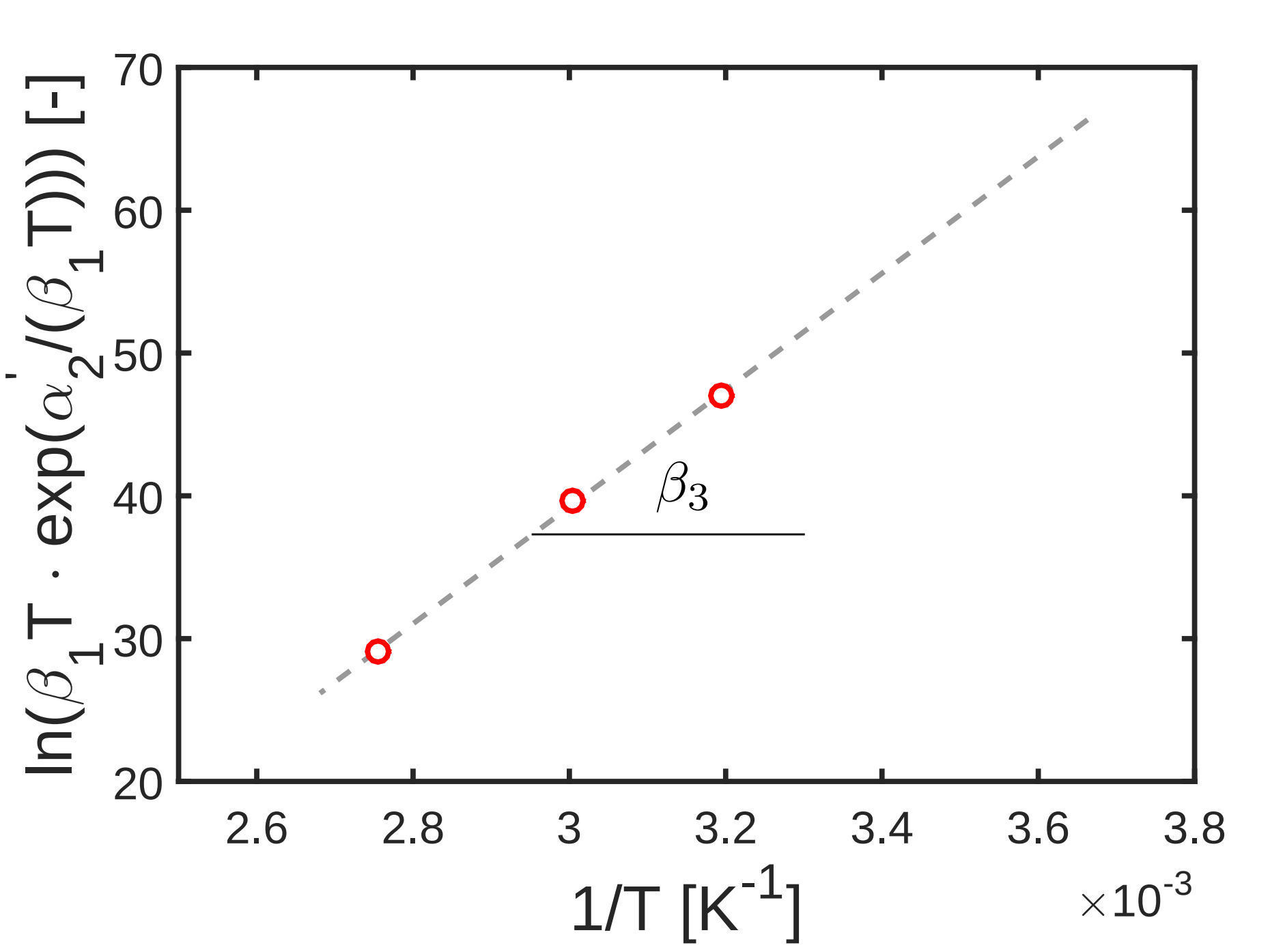
70
60
50
40
30
20
2.6
2.8
3
3.2
3.4
3.6
3.8
$\ln(\beta_1 T \cdot \exp(\alpha_2/(\beta_1 T)))$ [-]
1/T [K^{-1}]
$\times 10^{-3}$
β_3

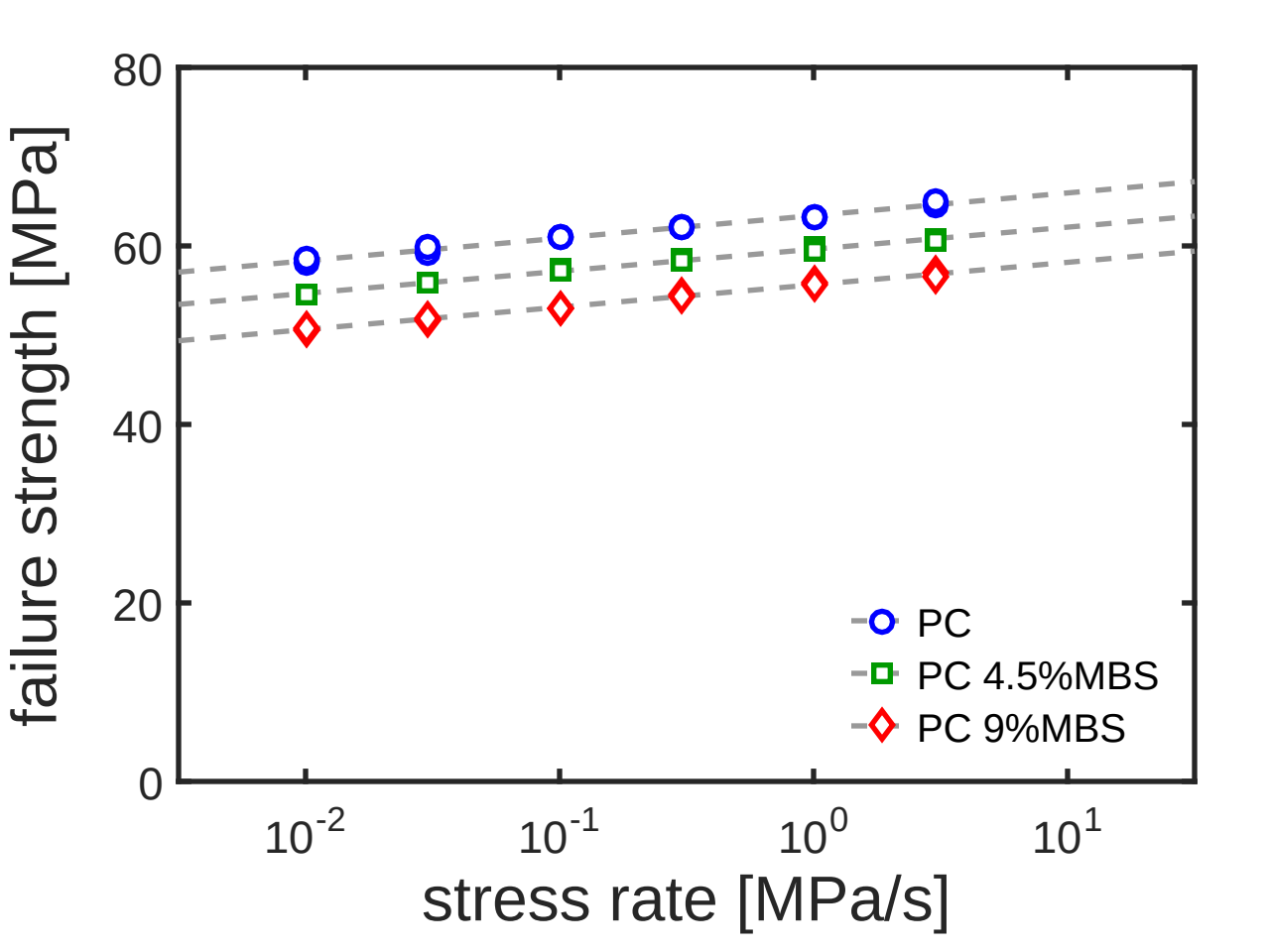
80
60
40
20
0
failure strength [MPa]
10^{-2}
10^{-1}
10^{0}
10^{1}
stress rate [MPa/s]
PC
PC 4.5%MBS
PC 9%MBS

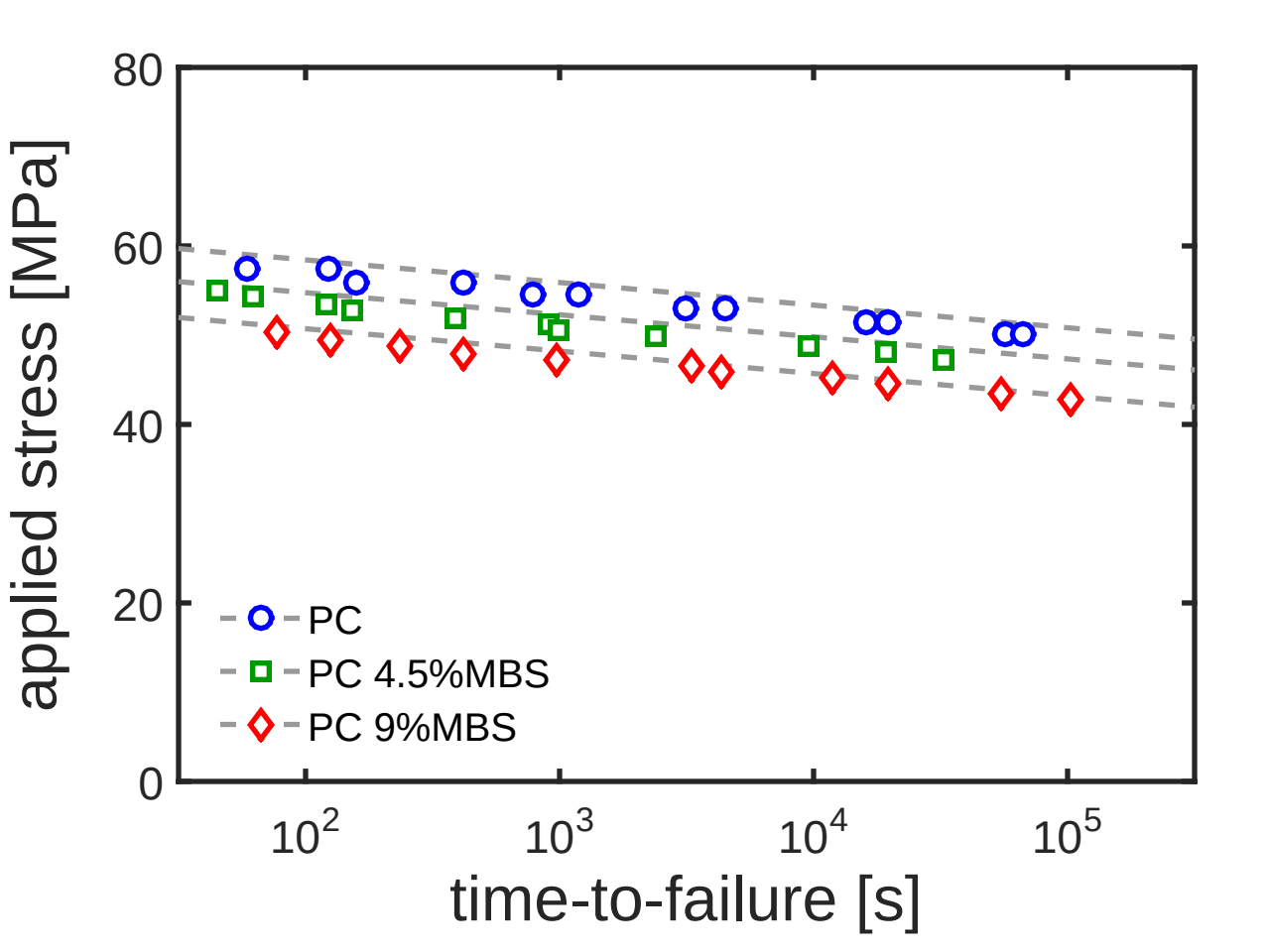
80
60
40
20
0
applied stress [MPa]
PC
PC 4.5%MBS
PC 9%MBS
10^2
10^3
10^4
10^5
time-to-failure [s]

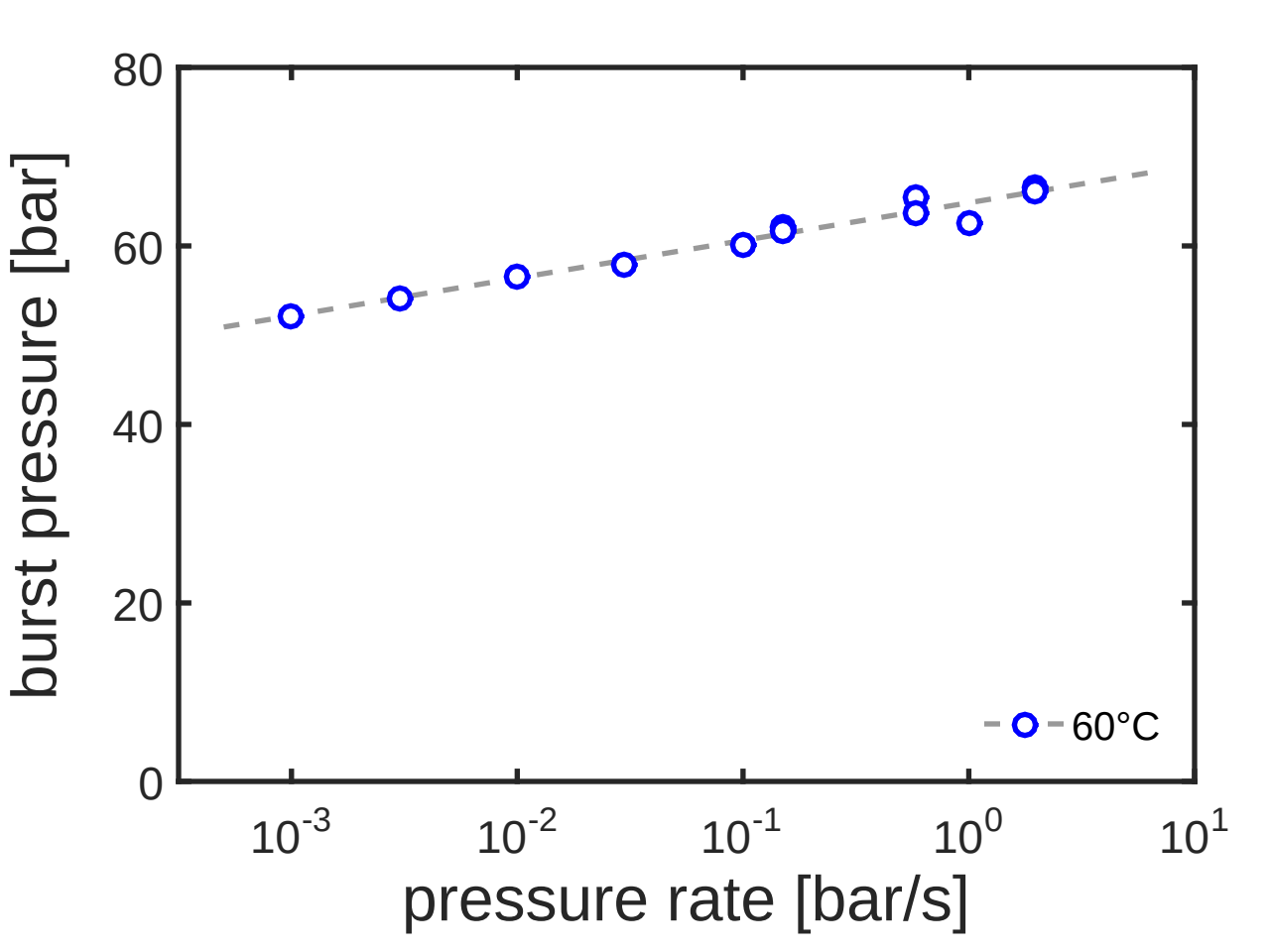
80
60
40
20
0
burst pressure [bar]
10^{-3}
10^{-2}
10^{-1}
10^{0}
10^{1}
pressure rate [bar/s]
60°C

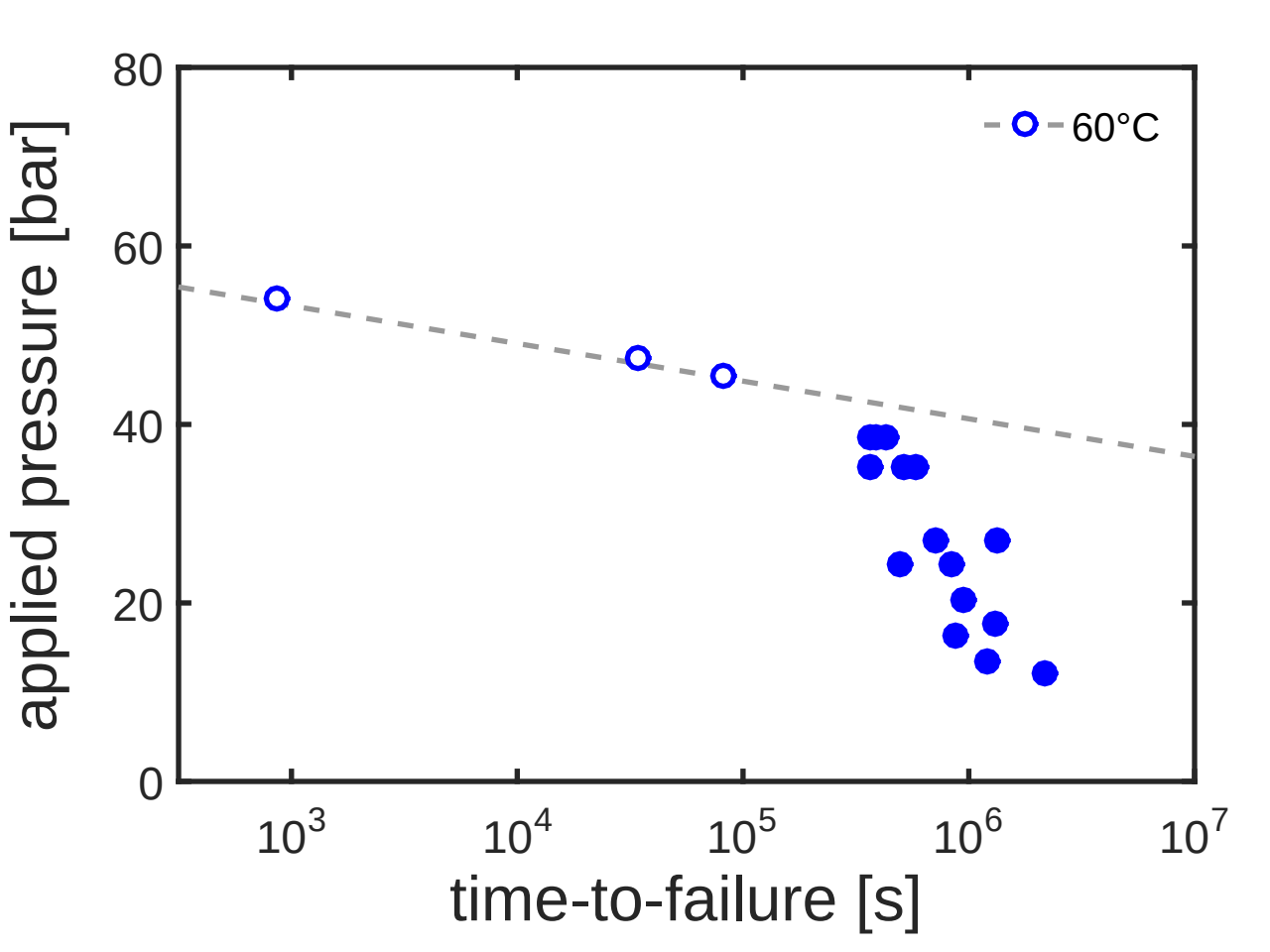
80
60
40
20
0
applied pressure [bar]
60°C
10^3
10^4
10^5
10^6
10^7
time-to-failure [s]

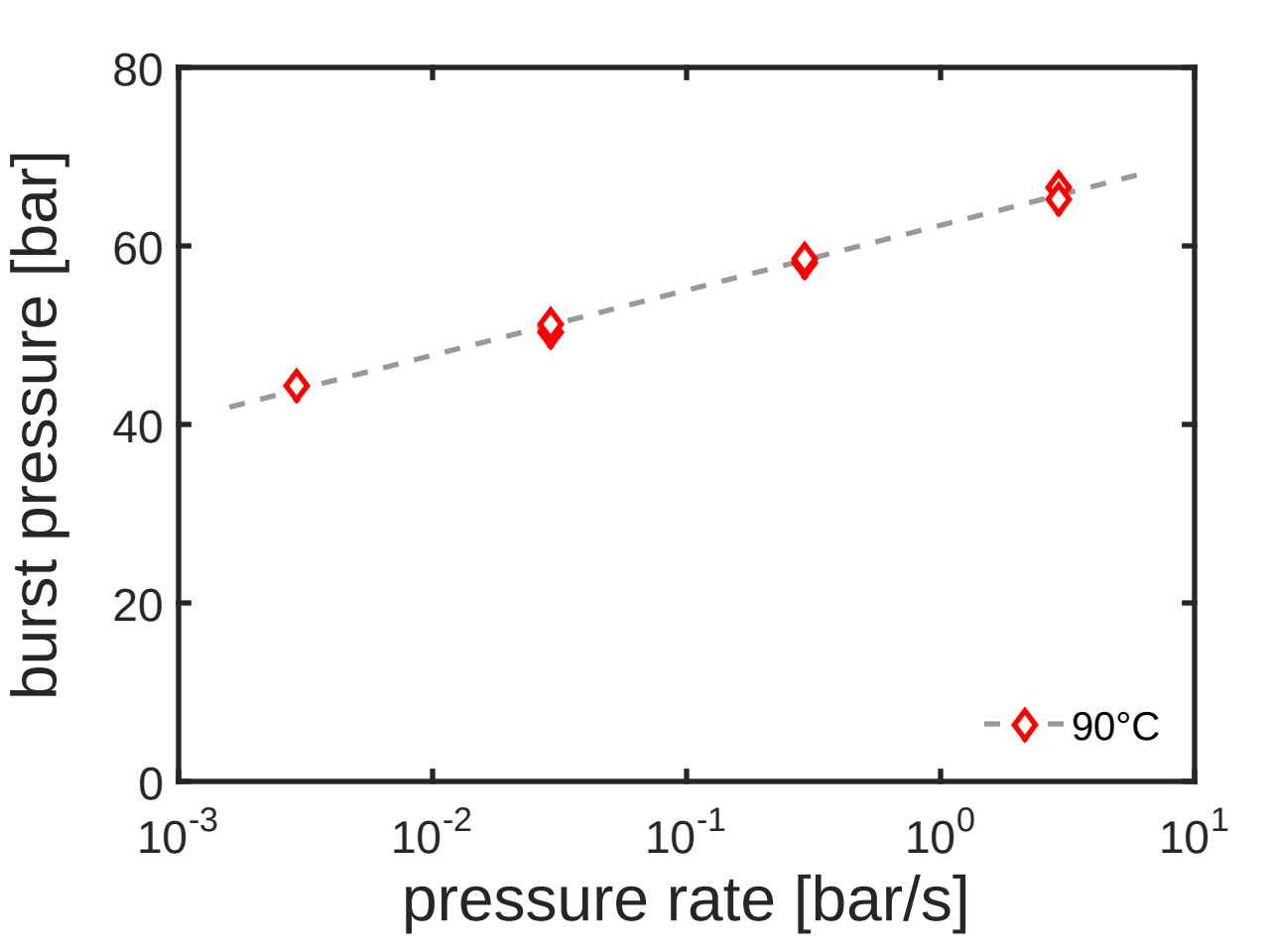
80
60
40
20
0
burst pressure [bar]
10^{-3}
10^{-2}
10^{-1}
10^{0}
10^{1}
pressure rate [bar/s]
90°C

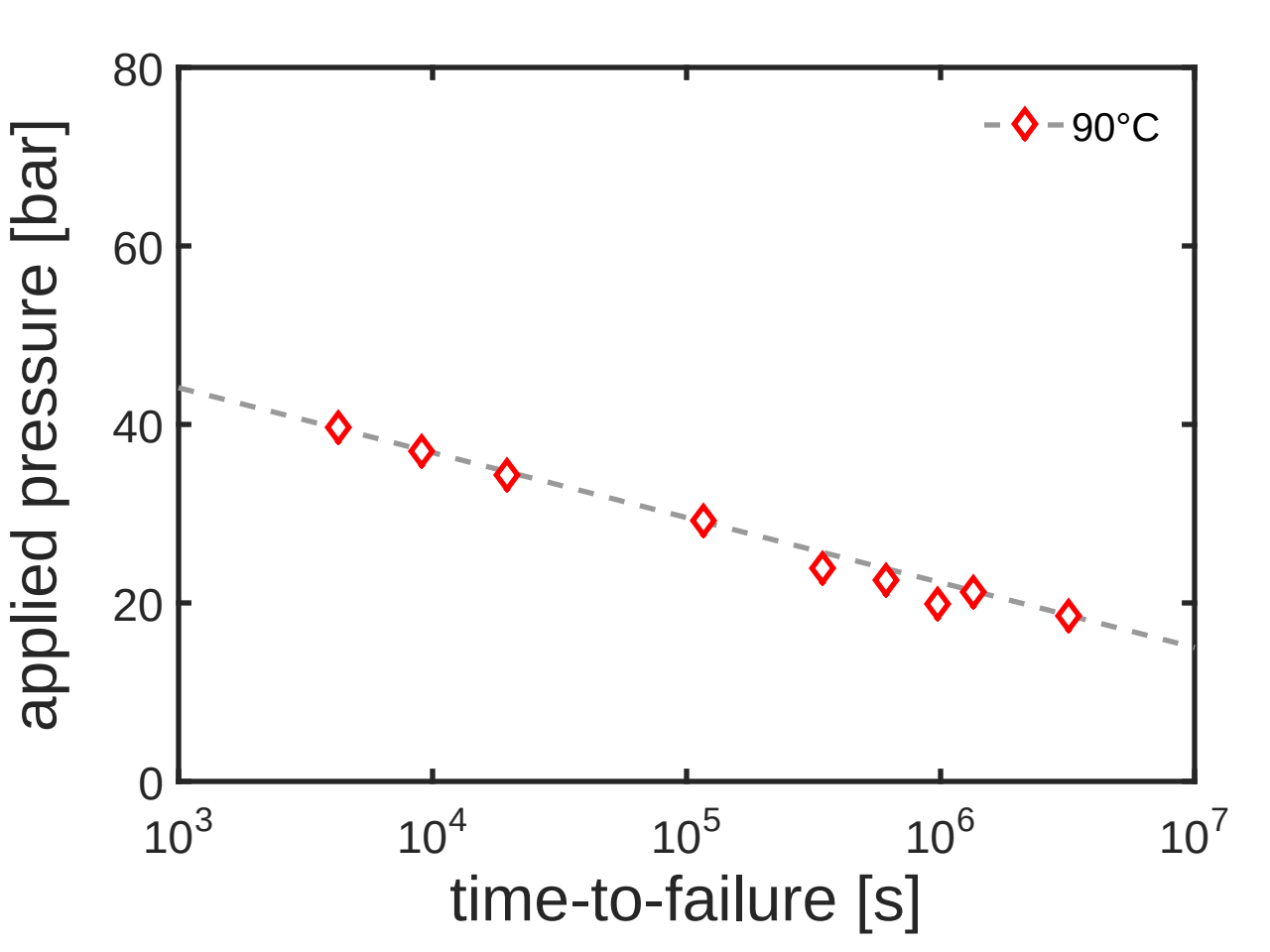
80
60
40
20
0
applied pressure [bar]
90°C
10^3
10^4
10^5
10^6
10^7
time-to-failure [s]

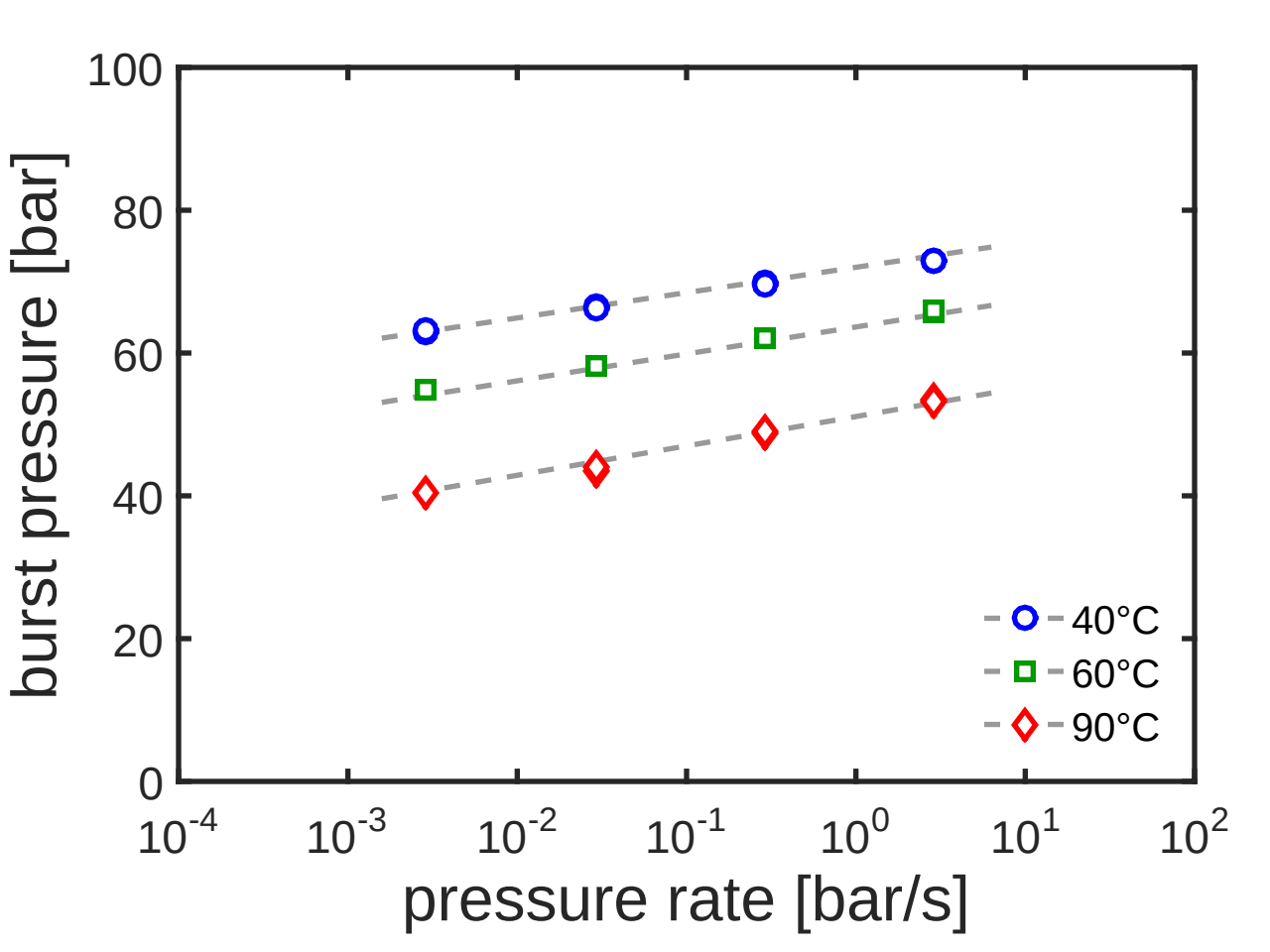
100
80
60
40
20
0
burst pressure [bar]
10-4
10-3
10-2
10-1
100
101
102
pressure rate [bar/s]
40°C
60°C
90°C

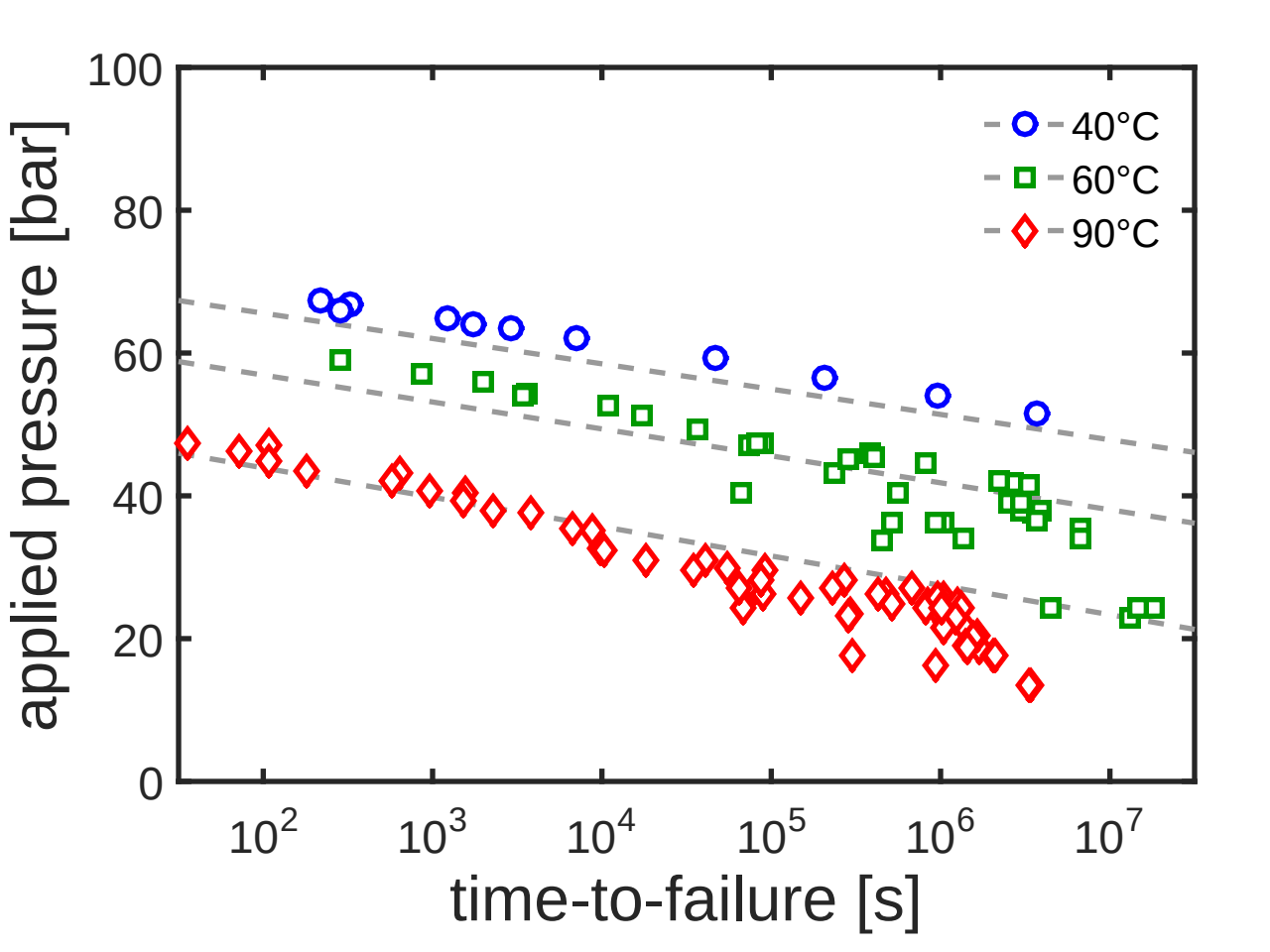
100
80
60
40
20
0
applied pressure [bar]
10^2
10^3
10^4
10^5
10^6
10^7
time-to-failure [s]
40°C
60°C
90°C

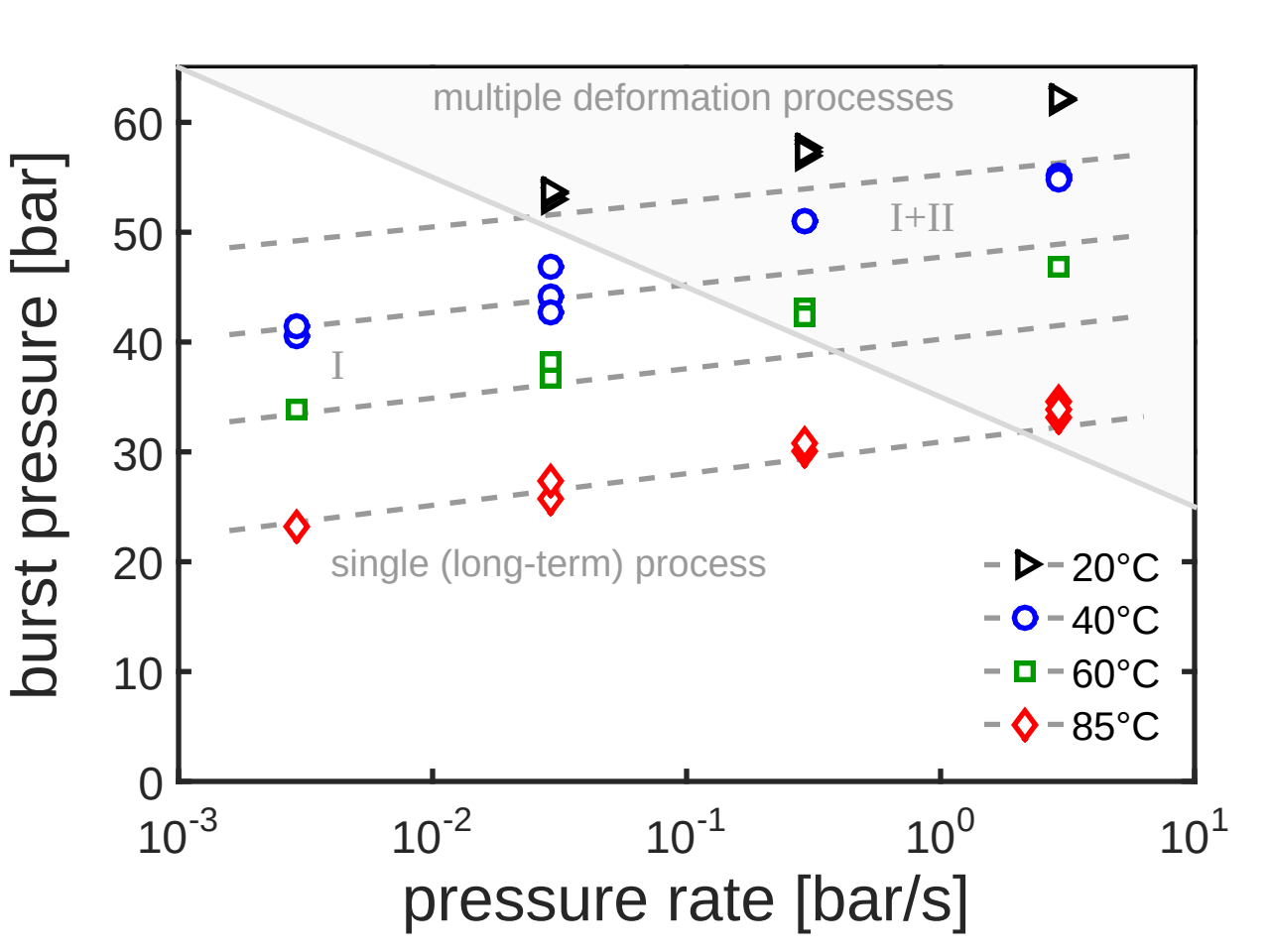
multiple deformation processes
I+II
I
single (long-term) process
20°C
40°C
60°C
85°C
burst pressure [bar]
pressure rate [bar/s]
0
10
20
30
40
50
60
10^-3
10^-2
10^-1
10^0
10^1

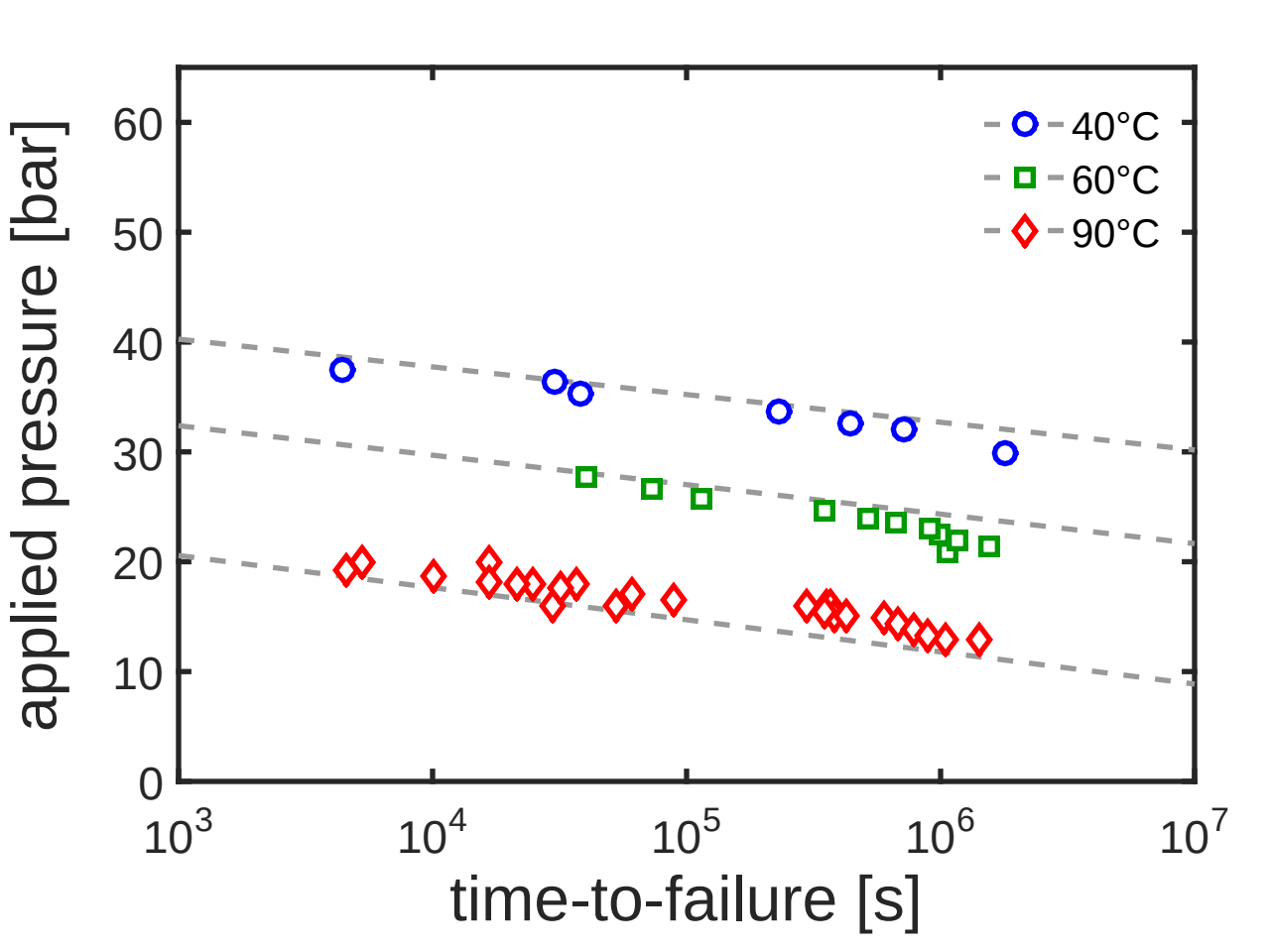
applied pressure [bar]
time-to-failure [s]
40°C
60°C
90°C
0
10
20
30
40
50
60
10^3
10^4
10^5
10^6
10^7